Fourier coefficients and moments of piecewise-circular curves

Alberto Ruiz[a,**]

[a] *DIS, University of Murcia, Spain*

ABSTRACT

Many natural and artificial shapes can be compactly described by sequences of circular arcs and straight line segments. This paper presents practical methods to compute the coefficients of the Fourier series of a piecewise-circular curve and the moments of the enclosed region. These descriptors are the basis of simple and widely used techniques for shape matching and alignment, that can now be efficiently applied to a more expressive data representation.

Keywords: piecewise curve, circular arc, Fourier descriptors, shape moments.

1. Introduction

Shape matching and alignment are important problems in visual pattern recognition (Zhang and Lu, 2004). Simple approaches involve Fourier descriptors (Zahn and Roskies, 1972; Persoon and Fu, 1977) and moments (Hu, 1962), which are useful to compute invariant features and alignment transformations (Sprinzak and Werman, 1994). Fourier coefficients are usually obtained by the FFT from regularly sampled contours, and moments are efficiently obtained from reduced polygonal approximations.

Many natural and artificial shapes can be accurately described by curves composed of linear and curved fragments (see Figs. 6 and 7). Depending on the amount of curvature and image resolution, the required number of fragments can be substantially less than the size of the raw digitized contour or a reduced polygon. This paper presents a simple and efficient method to extract Fourier and moment shape descriptors from this kind of compact curve model.

Smooth curves are usually modeled by expressive parametric families like Bezier curves or B-splines. However, for our present purposes, essential requirements are arc-length parameterization and efficient geometric transformations, since the detected shapes must often be normalized or aligned to templates. Of particular interest are the metric, affine, and projective transformation groups. Elliptic, fragments would be ideal, as conics transform into conics. Unfortunately, a natural arc-length parameterization of the ellipse is analytically unfeasible. As a practical alternative, in this paper we explore a representation based on circular arcs (Yang

*Corresponding author:
e-mail: aruiz@um.es (Alberto Ruiz)

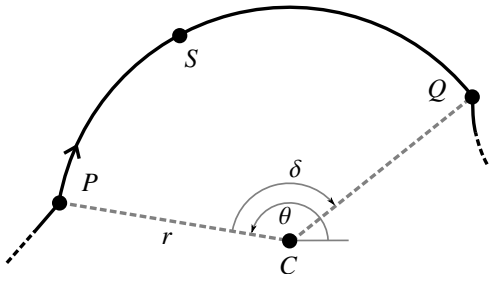

Fig. 1. Geometric description of an oriented circular arc.

and Du, 1996; Pei and Horng, 1996; Meek and Walton, 1992; Rosin and West, 1989; Tortorella et al., 2008; Kolesnikov, 2012; Kolesnikov and Kauranne, 2014).

The paper is organized as follows: Section 2 describes the proposed curve representation. In sections 3 and 4 we derive simple expressions for the Fourier coefficients and the shape moments. Section 5 analyzes the computational cost. Section 6 presents several illustrative experiments, and the final section summarizes the conclusions and future directions of this work.

2. Curve representation

Let $Z(t) \in \mathbb{C}$ be a curve defined piecewise by means of n sections $Z_k(t)$ for $t \in [t_k, t_{k+1})$, $k = 0 \ldots n-1$. Each section is either a proper circular arc with finite radius or a straight line segment.

Normalized arc-length is used as parameter so that the whole curve is traversed at constant speed for $t \in [0, 1)$. This parameterization is invariant to metric transformations and changes of the piecewise decomposition. This is essential to obtain consistent descriptors from different detected instances of the same object. (Affine invariance can also be achieved by a previous whitening transformation.)

2.1. Arcs

An oriented circular arc can be specified in many ways, using different subsets of geometric elements (Fig. 1). For example, we can use an ordered triplet (P, S, Q) with the starting point P, the final point Q, and some intermediate point S. The center C and direction of traversal, or some measure of curvature, can be given instead of S.

A minimal specification is (P, Q, δ), including the extremes and the signed angular displacement $\delta \in (-2\pi, +2\pi)$, which fixes both length and direction of traversal (Fig. 2). Null curvature, with $\delta = 0$, indicates a linear segment. From (P, Q, δ) we obtain the center C, radius r, and absolute angle θ of the initial point. Arc length is $l = |r\delta|$ and the extremes can be written as

$$P = C + re^{i\theta}, \qquad Q = C + re^{i(\theta+\delta)}. \tag{1}$$

In addition to the geometric features of the constituent arcs, we also need the values of the parameter t at the extremes. Let $L = \sum_k l_k$ be the length of the whole curve. For the k-th arc we obtain the normalized length $\tau_k = l_k/L$ and the initial parameter

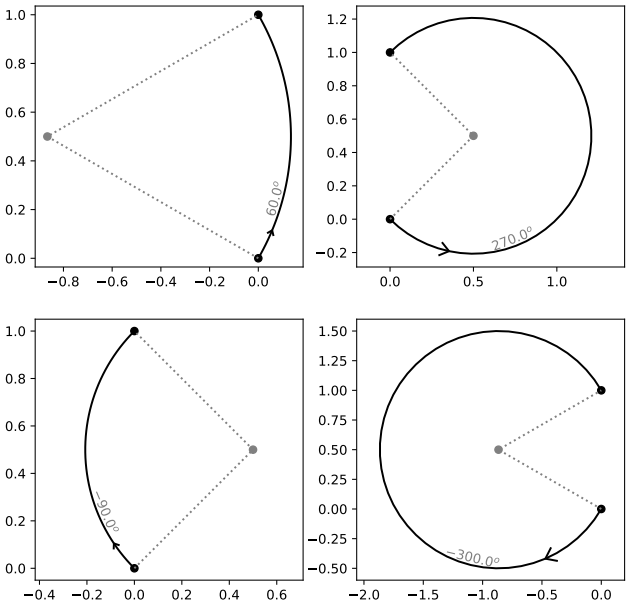

Fig. 2. Oriented arcs from (0,0) to (0,1) for several values of δ.

Table 1. Extended representation of the test curve in Fig 3.

k	t_k	τ	P		Q		C		r	δ	v	υ	
0	0.000	0.332	0.3	0.0	1.0	0.2	0.53	0.52	0.566	1.396	4.200		
1	0.332	0.516	1.0	0.2	0.0	-0.2	0.33	0.42	0.703	-1.745	-3.383		
2	0.848	0.152	0.0	-0.2	0.3	0.0						1.979	1.319

$t_k = \sum_{j<k} \tau_j$, so that $P_k = Z(t_k)$ and $Q_k = Z(t_k + \tau_k) = P_{k+1} = Z(t_{k+1})$. Finally, we obtain the angular speed $v_k = \frac{\delta_k}{\tau_k}$. Both t_k and τ_k depend on all the pieces of the curve and must be computed in a preprocessing step.

All subsequent computations can be concisely expressed in terms of the following extended representation of the arcs as parts of a curve:

$$\mathcal{A}_k = (P, Q, C, r, \theta, \delta, t_k, \tau, v) \tag{2}$$

(For clarity of notation, we omit the index k in a variable if there is no risk of confusion.)

2.2. Straight line segments

The special case of a straight path is specified by the extremes and the linear velocity $\upsilon = \frac{Q-P}{\tau}$.

$$\mathcal{S}_k = (P, Q, t_k, \tau, \upsilon) \tag{3}$$

Fig. 3 shows the minimal description of a simple test curve composed of three sections, and Table 1 shows the corresponding extended representation.

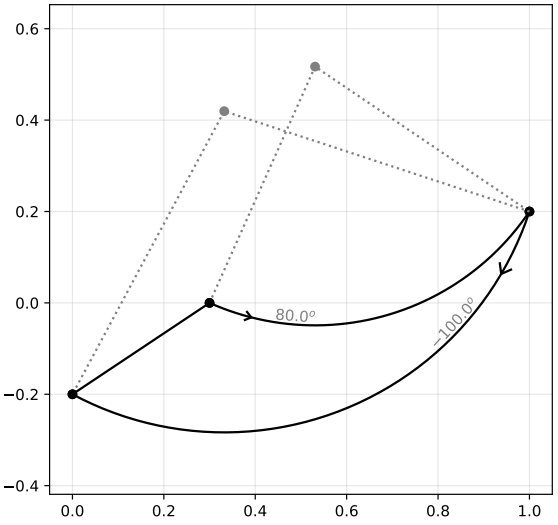

k	P		δ
0	0.3	0.0	1.396
1	1.0	0.2	-1.745
2	0.0	-0.2	0

Fig. 3. Test curve.

2.3. Union and subdivision of arcs

The above representation is suitable for efficient fusion of consecutive arcs and division of one arc into fragments. These operations are needed for curve transformation and simplification.

Two consecutive arcs with common center also share radius and angular speed, so $\mathcal{A}_1 = (P, S, C, r, \theta, \delta_1, t_0, \tau_1, v)$ and $\mathcal{A}_2 = (S, Q, C, r, \cdot, \delta_2, \cdot, \tau_2, v)$ are equivalent to $\mathcal{A} = (P, Q, C, r, \theta, \delta_1 + \delta_2, t_0, \tau_1 + \tau_2, v)$.

Reciprocally, $\mathcal{A} = (P, Q, C, r, \theta, \delta, t_0, \tau, v)$ can be divided into two consecutive fragments $\mathcal{A}_1 = (P, D, C, r, \theta, \delta\gamma, t_0, \tau\gamma, v)$ and $\mathcal{A}_2 = (D, Q, C, r, t_0 + \tau\gamma, \delta(1-\gamma), \theta + \delta\gamma, \tau(1-\gamma), v)$ at any point $D = C + r^{i(\theta+\delta\gamma)}$ located at a given proportion of length $\gamma \in (0, 1)$.

The union and division of line segments is also immediate.

Other curve sections are not affected by these operations.

2.4. Transformation of arcs

Circular arcs are also very convenient for the implementation of curve transformations.

Metric transformations preserve angles and ratios of distances, so in the extended representation we must only transform P, Q, and C, scale r, and update θ.

Affine and projective transformations distort circles into ellipses, which can be accurately approximated by circular arcs (Rosin, 1999; Chandrupatla and Osler, 2008). Therefore, arcs can be efficiently warped by subdivision and transformation of the extremes and a few intermediate points. In this case the preprocessing step must be redone to update the parameterization, but the whole

Table 2. Selected $F_k(\omega)$ terms of the test curve (real and imaginary parts).

k	$F_k(-3)$		$F_k(-2)$		$F_k(-1)$		$F_k(0)$		$F_k(1)$		$F_k(2)$		$F_k(3)$	
0	0.008	-0.031	-0.082	0.045	0.054	0.172	0.224	0.005	0.068	-0.188	-0.104	-0.068	-0.015	0.048
1	0.011	0.062	0.111	-0.013	-0.285	0.023	0.290	-0.079	-0.144	0.031	0.042	0.055	0.007	-0.048
2	-0.000	-0.010	0.004	-0.016	0.012	-0.019	0.023	-0.015	0.030	-0.005	0.030	0.008	0.022	0.019

process is much faster than the explicit transformation of a densely sampled sequence of points, which must also be uniformly resampled again if the FFT is to be used.

The number of divisions required to achieve a given accuracy depends on the curvature of the arc, and also on the amount deformation, as illustrated in Fig. 4.

Fig. 4. Transformation of arcs via subdivision. Left: original curve. Center: two divisions per arc, not enough for high curvature sections. Right: four divisions per arc.

3. Fourier coefficients

The coefficient $F(\omega)$ of the Fourier series of a curve $Z(t) \in \mathbb{C}$, defined piecewise on $t \in [0, 1)$ as described above, and extended periodically outside, is the sum of contributions of each fragment:

$$F(\omega) = \int_0^1 Z(t) e^{-i2\pi\omega t} dt = \sum_{k=0}^{n-1} F_k(\omega), \tag{4}$$

where

$$F_k(\omega) \equiv \int_{t_k}^{t_{k+1}} Z_k(t) e^{-i2\pi\omega t} dt. \tag{5}$$

In this section we derive simple expressions for $F_k(\omega)$.

3.1. Circular arc

Let $H_k \equiv e^{-i2\pi t_k}$. For $Z_k(t) \sim (P, Q, C, r, \theta, \delta, t_k, \tau, v)$, the term $F_k(\omega)$ can be written as

$$F_k(\omega) = \alpha(\omega, Q)\ H^{\omega}_{k+1} - \alpha(\omega, P)\ H^{\omega}_{k}, \tag{6}$$

where

$$\alpha(\omega, x) = \frac{i(x - C)}{2\pi\omega - v} + \frac{i\ C}{2\pi\omega} \tag{7}$$

Proof. This section of the curve can be parameterized as

$$Z_k(t) = C + re^{i(vt+b)}, \quad t \in [t_k, t_{k+1}), \tag{8}$$

with $b = \theta - vt_k$, so that

$$\begin{aligned} vt_k + b &= \theta, & P - C &= re^{ib}e^{vt_k} \\ vt_{k+1} + b &= \theta + \delta, & Q - C &= re^{ib}e^{vt_{k+1}} \end{aligned} \tag{9}$$

Then (5) becomes

$$F_k(\omega) = C\int_{t_k}^{t_{k+1}} e^{-i2\pi\omega t}dt \;+\; re^{ib}\int_{t_k}^{t_{k+1}} e^{-i(2\pi\omega - v)t}dt \tag{10}$$

The first integral is immediate:

$$C\int_{t_k}^{t_{k+1}} e^{-i2\pi\omega t}dt = \frac{iC}{2\pi\omega}(H^\omega_{k+1} - H^\omega_k). \tag{11}$$

The second one is also very simple and can be compactly expressed in terms of the arc extremes:

$$\begin{aligned} re^{ib}\int_{t_k}^{t_{k+1}} e^{-i(2\pi\omega - v)t}dt &= \frac{ire^{ib}}{2\pi\omega - v}\left(e^{ivt_{k+1}}H^\omega_{k+1} - e^{ivt_k}H_k\omega\right) = \\ &= \frac{i}{2\pi\omega - v}\left((Q-C)H^\omega_{k+1} - (P-C)H^\omega_k\right). \end{aligned} \tag{12}$$

Eq. (7) follows directly from rearrangement of (11) and (12).

□

There are two special cases of (10) not covered by (7). For $\omega = 0$ it reduces to

$$\begin{aligned} F_k(0) &= C\int_{t_k}^{t_{k+1}} dt \;+\; re^{ib}\int_{t_k}^{t_{k+1}} e^{ivt}dt = \\ &= C\tau + re^{ib}\frac{1}{iv}(e^{ivt_{k+1}} - e^{ivt_k}) = C\tau + \frac{Q-P}{iv}, \end{aligned} \tag{13}$$

and for $v = 2\pi\omega$ we have

$$
\begin{aligned}
F_k(\omega) &= C \int_{t_k}^{t_{k+1}} e^{-i2\pi\omega t} dt \;+\; re^{ib} \int_{t_k}^{t_{k+1}} dt = \\
&= \frac{iC}{2\pi\omega}(H^{\omega}_{k+1} - H^{\omega}_{k}) + \tau r e^{ib} = \\
&= \frac{iC}{2\pi\omega}(H^{\omega}_{k+1} - H^{\omega}_{k}) + \tau \frac{P - C}{e^{i\upsilon t_k}}
\end{aligned} \tag{14}
$$

3.2. Straight line segment

For $Z_k(t) \sim (P, Q, t_k, \tau, \upsilon)$ the contribution $F_k(\omega)$ can also be written as (6), with

$$
\alpha(\omega, x) = \frac{ix}{2\pi\omega} + \frac{\upsilon}{4\pi^2\omega^2} \tag{15}
$$

and the special case

$$
F_k(0) = \frac{P + Q}{2}\, \tau. \tag{16}
$$

Proof. Eq. (15) follows directly from the parameterization

$$
Z_k(t) = \upsilon t + b, \quad t \in [t_k, t_{k+1}), \tag{17}
$$

and the elementary integral

$$
\int (\upsilon t + b)\, e^{at} dt = \frac{1}{a}\left(\upsilon t + b - \frac{\upsilon}{a}\right) e^{at}, \tag{18}
$$

with $\upsilon t_k + b = P$, $\upsilon t_{k+1} + b = Q$, and $a = -i2\pi\omega$. The special case $\omega = 0$ is also immediate.

□

Table 2 shows the numeric values of a few $F_k(\omega)$ terms for the testing curve in Fig 3. From the raw Fourier coefficients any standard invariant descriptor can be readily obtained.

Remark. For piecewise-linear functions it is customary to group the $\alpha(\omega, \cdot)$ terms of consecutive segments, canceling the contributions of $Q_k = P_{k+1}$ in (15), and producing a simple expression in terms of the curvature $\upsilon_k - \upsilon_{k-1}$ at each node (Burkhardt, 2007). An analogous (although not so simple) grouping could be developed for consecutive arcs but it is less useful as the curve freely combines arcs and segments with four possible kinds of path junctions at each node.

3.3. Norm

The vector of coefficients of a truncated Fourier series $\mathcal{F}_\Omega = \{F_\omega\}$ with $|\omega| \leq \Omega$ is a compact, low-pass representation of a continuous curve using $2\Omega + 1$ complex numbers. To be useful in practice we need information about the accuracy of the approximation, that can be quantified by the norm ϵ of the discarded terms. From Parseval's Theorem,

$$|Z(t)|^2 = \int_0^1 \overline{Z}(t)Z(t)dt = \sum_{\omega=-\infty}^{+\infty} |F_\omega|^2 = |\mathcal{F}_\Omega|^2 + \epsilon^2. \tag{19}$$

The norm $|Z(t)|^2$ can be easily computed as the sum of simple contributions from each fragment:

$$|Z(t)|^2 = \int_0^1 \overline{Z}(t)Z(t)dt \equiv \sum_{k=0}^{n-1} \mathcal{N}_k^2 \tag{20}$$

For arcs:

$$\begin{aligned} \mathcal{N}_k^2 &= \int_{t_k}^{t_{k+1}} |C + re^{i(vt+b)}|^2 dt = \\ &= \left(|C|^2 + r^2\right)\tau + \frac{2}{a}\mathrm{Im}\left((Q-P)\overline{C}\right). \end{aligned} \tag{21}$$

For segments:

$$\begin{aligned} \mathcal{N}_k^2 &= \int_{t_k}^{t_{k+1}} |vt + b|^2 dt = \\ &= \left[\frac{|v|^2}{3}t^3 + \mathrm{Re}\left(v\overline{b}\right)t^2 + |b|^2 t\right]_{t_k}^{t_{k+1}}. \end{aligned} \tag{22}$$

Table 3 shows the numeric values of the contributions to the norm of the test curve in Fig. 3.

Table 3. Contributions to the norm.

k	$\lvert Z_k(t)\rvert^2$
0	0.16738
1	0.23321
2	0.00657

A normalized measure of preservation of shape details in the approximation, independent of position and size, is given by the following ratio, taking into account the frequency components above the basic elliptic model given by $\mathcal{F}_1$.

$$\xi^2 \equiv \frac{|\mathcal{F}_\Omega|^2 - |\mathcal{F}_1|^2}{|Z(t)|^2 - |\mathcal{F}_1|^2} \tag{23}$$

Table 4. Contributions to the second order moments.

k	m_{00}	m_{10}	m_{01}	m_{20}	m_{02}	m_{11}
0	0.09597	0.04019	0.00853	0.02111	0.00123	0.00373
1	-0.28792	-0.11776	0.01449	-0.06437	-0.00531	0.00425
2	0.03000	0.00300	-0.00200	0.00045	0.00020	-0.00015

4. Moments

The moments of a planar region enclosed by a piecewise-circular curve can also be obtained from the extended description proposed in Section 2. Here we change to a real representation $Z(t) = (x(t), y(t)) \in \mathbb{R}^2$. Using Green's Theorem the raw moments can again be expressed as a sum of contributions from each fragment:

$$\begin{aligned} m_{pq} &\equiv \iint_{\mathcal{S}} x^p y^q dxdy = \frac{1}{2} \oint_Z \left[\frac{x^p y^{q+1}}{q+1} dx - \frac{x^{p+1} y^q}{p+1} dy \right] \\ &= \frac{1}{2(q+1)} \sum_{k=0}^{n-1} A_k - \frac{1}{2(p+1)} \sum_{k=0}^{n-1} B_k, \end{aligned} \tag{24}$$

where

$$A_k = \int_{t_k}^{t_{k+1}} \left(x(t)^p y(t)^{q+1} \frac{dx}{dt} \right) dt \tag{25}$$

$$B_k = \int_{t_k}^{t_{k+1}} \left(x(t)^{p+1} y(t)^q \frac{dy}{dt} \right) dt. \tag{26}$$

4.1. Circular arc

For an arc section $Z_k(t) \sim (P, Q, C, r, \theta, \delta, t_k, \tau, v)$, parameterized as $x(t) = c_x + r\cos(t)$, $y(t) = c_y + r\sin(t)$, with $t \in [\theta, \theta + \delta)$, and $C = (c_x, c_y)$, we get

$$A_k = \int_{\theta}^{\theta+\delta} \Big((c_x + r\cos(t))^p (c_y + r\cos(t))^{q+1} (-r\sin(t)) \Big) dt \tag{27}$$

$$B_k = \int_{\theta}^{\theta+\delta} \Big((c_x + r\cos(t))^{p+1} (c_y + r\cos(t))^q (r\cos(t)) \Big) dt. \tag{28}$$

Expanding powers we obtain a linear combination of integrals of the form

$$T_{m,n} = \int \sin^m(t) \cos^n(t) dt, \tag{29}$$

that can be evaluated by means of a reduction formula (Wikipedia contributors, 2018):

$$T_{m,n} = \begin{cases} -\frac{\sin^{m-1}(t)\cos^{n+1}(t)}{m+n} + \frac{m-1}{m+n} T_{m-2,n} \\ \frac{\sin^{m+1}(t)\cos^{n-1}(t)}{(m+n)} + \frac{n-1}{m+n} T_{m,n-2} \end{cases} \tag{30}$$

Therefore, any moment of a region with a piecewise-circular boundary can be automatically computed by a recursive algorithm. However, simpler explicit expressions are convenient for the widely used lower order moments. Let us denote the centered extremes of the arc as $(x_1, y_1) \equiv P - C = (r\cos(\theta), r\sin(\theta))$, and $(x_2, y_2) \equiv Q - C = (r\cos(\theta+\delta), r\sin(\theta+\delta))$. With the help of the symbolic algebra software `sympy` (Meurer et al., 2017) we can derive the following formulas for the contributions of each fragment:

$$2\,m_{00} = \delta r^2 - c_x y_1 + c_x y_2 + c_y x_1 - c_y x_2 \tag{31}$$

$$\begin{aligned} 12\,m_{10} = {} & 6\delta c_x r^2 - 3c_x^2 y_1 + 3c_x^2 y_2 + 6c_x c_y x_1 - 6c_x c_y x_2 + \\ & + 3c_y x_1^2 - 3c_y x_2^2 - 3x_1^2 y_1 + 3x_2^2 y_2 - 4y_1^3 + 4y_2^3 \end{aligned} \tag{32}$$

$$\begin{aligned} 12\,m_{01} = {} & 6\delta c_y r^2 - 6c_x c_y y_1 + 6c_x c_y y_2 + 3c_x x_1^2 - 3c_x x_2^2 + \\ & + 3c_y^2 x_1 - 3c_y^2 x_2 + 4x_1^3 + 3x_1 y_1^2 - 4x_2^3 - 3x_2 y_2^2 \end{aligned} \tag{33}$$

$$\begin{aligned} 24\,m_{20} = {} & 12\delta c_x^2 r^2 + 3\delta x_2^4 + 6\delta x_2^2 y_2^2 + 3\delta y_2^4 - 4c_x^3 y_1 + 4c_x^3 y_2 + \\ & + 12c_x^2 c_y x_1 - 12c_x^2 c_y x_2 - 12c_x c_y y_1^2 + 12c_x c_y y_2^2 - 12c_x x_1^2 y_1 + \\ & + 12c_x x_2^2 y_2 - 16c_x y_1^3 + 16c_x y_2^3 + 4c_y x_1^3 - 4c_y x_2^3 - \\ & - x_1^3 y_1 - 3x_1 y_1^3 + x_2^3 y_2 + 3x_2 y_2^3 \end{aligned} \tag{34}$$

$$\begin{aligned} 24\,m_{02} = {} & 12\delta c_y^2 r^2 + 3\delta x_2^4 + 6\delta x_2^2 y_2^2 + 3\delta y_2^4 - 12c_x c_y^2 y_1 + \\ & + 12c_x c_y^2 y_2 - 12c_x c_y y_1^2 + 12c_x c_y y_2^2 - 4c_x y_1^3 + 4c_x y_2^3 + \\ & + 4c_y^3 x_1 - 4c_y^3 x_2 + 16c_y x_1^3 + 12c_y x_1 y_1^2 - 16c_y x_2^3 - \\ & - 12c_y x_2 y_2^2 + 3x_1^3 y_1 + x_1 y_1^3 - 3x_2^3 y_2 - x_2 y_2^3 \end{aligned} \tag{35}$$

$$
\begin{aligned}
48\, m_{11} = {} & 24\delta c_x c_y r^2 - 12 c_x^2 c_y y_1 + 12 c_x^2 c_y y_2 - 6 c_x^2 y_1^2 + 6 c_x^2 y_2^2 + \\
& + 12 c_x c_y^2 x_1 - 12 c_x c_y^2 x_2 + 16 c_x x_1^3 + 12 c_x x_1 y_1^2 - 16 c_x x_2^3 - \\
& - 12 c_x x_2 y_2^2 - 6 c_y^2 y_1^2 + 6 c_y^2 y_2^2 - 12 c_y x_1^2 y_1 + 12 c_y x_2^2 y_2 - \\
& - 16 c_y y_1^3 + 16 c_y y_2^3 + 3 x_1^4 - 3 x_2^4 - 3 y_1^4 + 3 y_2^4
\end{aligned} \tag{36}
$$

4.2. Straight line segment

For a linear section $Z_k(t) \sim (P, Q, t_k, \tau, v)$ we use the parameterization $Z(t) = P + (Q - P)t$, for $t \in [0, 1)$. Let $P = (x_1, y_1)$, $Q = (x_2, y_2)$, $\Delta x = x_2 - x_1$, and $\Delta y = y_2 - y_1$. It can be shown (Ruiz et al., 2017) that

$$
\begin{aligned}
A_k &= \Delta x\, I_{p,q+1}(x_1, \Delta x, y_1, \Delta y) \\
B_k &= \Delta y\, I_{p+1,q}(x_1, \Delta x, y_1, \Delta y)
\end{aligned} \tag{37}
$$

where

$$
\begin{aligned}
I_{n,m}(x, u, y, v) &\equiv \int_0^1 (x + ut)^n (y + vt)^m dt = \\
&= \sum_{j=0}^{n} \sum_{k=0}^{m} \binom{n}{j} \binom{m}{k} \frac{x^j u^{n-j} y^k v^{m-k}}{n + m - j - k + 1}.
\end{aligned} \tag{38}
$$

The terms for the moments up to second order are shown for comparison with the expressions for circular arcs.

$$
2\, m_{00} = x_1 y_2 - x_2 y_1 \tag{39}
$$

$$
\begin{aligned}
12\, m_{10} = {} & x_1^2 y_1 + 2 x_1^2 y_2 - 2 x_1 x_2 y_1 + \\
& + 2 x_1 x_2 y_2 - 2 x_2^2 y_1 - x_2^2 y_2
\end{aligned} \tag{40}
$$

$$
\begin{aligned}
12\, m_{01} = {} & -x_1 y_1^2 + 2 x_1 y_1 y_2 + 2 x_1 y_2^2 - \\
& - 2 x_2 y_1^2 - 2 x_2 y_1 y_2 + x_2 y_2^2
\end{aligned} \tag{41}
$$

$$12\,m_{20} = x_1^3 y_1 + x_1^3 y_2 - x_1^2 x_2 y_1 + x_1^2 x_2 y_2 - \\ - x_1 x_2^2 y_1 + x_1 x_2^2 y_2 - x_2^3 y_1 - x_2^3 y_2 \tag{42}$$

$$12\,m_{02} = -x_1 y_1^3 + x_1 y_1^2 y_2 + x_1 y_1 y_2^2 + x_1 y_2^3 - \\ - x_2 y_1^3 - x_2 y_1^2 y_2 - x_2 y_1 y_2^2 + x_2 y_2^3 \tag{43}$$

$$24\,m_{11} = 2x_1^2 y_1 y_2 + x_1^2 y_2^2 - 2x_1 x_2 y_1^2 + \\ + 2x_1 x_2 y_2^2 - x_2^2 y_1^2 - 2x_2^2 y_1 y_2 \tag{44}$$

Table 4 shows the numeric values of above terms for the test curve. Derived features such as the mean and the covariance coefficients, useful for shape normalization, are directly obtained from the raw moments:

$$\begin{aligned} \eta_{pq} &= m_{pq}/m_{00} \\ \mu_x &= \eta_{10} \\ \mu_y &= \eta_{01} \\ \sigma_x^2 &= \eta_{20} - \mu_x^2 \\ \sigma_y^2 &= \eta_{02} - \mu_y^2 \\ \sigma_{xy} &= \eta_{11} - \mu_x \mu_y \end{aligned} \tag{45}$$

Remark. The location and scale parameters derived from the computationally cheaper elliptic approximation $\mathcal{F}_1$ of a curve are not suitable for affine normalization. They in general differ from the moments of the enclosed area (Fig. 5).

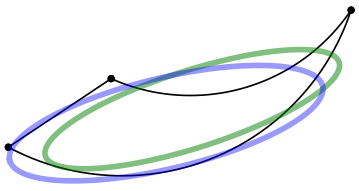

Fig. 5. Comparison of the $\mathcal{F}_1$ elliptic approximation of the test curve (green) and the covariance ellipse of the enclosed region (blue).

Higher order moments, useful for construction of invariants (Hu, 1962) and canonicalization (Ruiz et al., 2017), are not included here for lack of space but are available online (see Section 6.1).

5. Computational complexity.

Due to the similar mathematical nature of the circular arcs and the Fourier basis, the proposed curve representation does not introduce any computational overhead: the cost of an arc (7) is comparable to that of a linear segment (15).

The standard FFT is extremely efficient, but it requires dense uniform resampling to accurately model convoluted shapes, introducing appreciable overhead for normalization and alignment transformations. Therefore, a piecewise-circular model is competitive if the curve can be accurately described by a moderate number of arcs and segments and, as usual, only a few low-frequency coefficients are required.

Regarding the moments, Table 5 shows the computational cost of the first and second order moments, as measured by the number of terms per fragment. A circular arc is less than 3 times as costly (88 terms) as a linear segment (36 terms). Therefore, when approximating a digitized curve, if the prescribed tolerance is satisfied, it is generally favorable to introduce a circular arc instead of three or more segments.

Table 5. Number of terms per fragment for m_{pq}

p,q	linear	arc
0,0	2	5
1,0	6	11
0,1	6	11

p,q	linear	arc
2,0	8	20
0,2	8	20
1,1	6	21

6. Experiments

In this section we verify the derived formulas and discuss the advantages of the proposed approach. Fig. 6 shows simple synthetic curves together with their corresponding low frequency reconstructions from truncated series. The moments of each enclosed region are displayed by means of an ellipse with the same mean and covariance matrix (Safaee-Rad et al., 1992). The results are fully consistent with those of the standard FFT and moment algorithms working on densely sampled curves. Shape normalization is illustrated in the bottom-right case. It shows a whitened version of the test shape, transformed as described in Sect. 2.4 to get a circular covariance ellipse.

Fig. 7 shows a similar analysis of digitized contours taken from natural images. The Fourier coefficients and moments are efficiently computed from piecewise-circular approximations obtained by a simple greedy extension of the method of Douglas and Peucker (1973): for each recursive subdivision of the curve, if a linear piece cannot be fitted we try the arc defined by the extremes and the furthest point. Though not optimal, it reduces considerably the number of fragments.

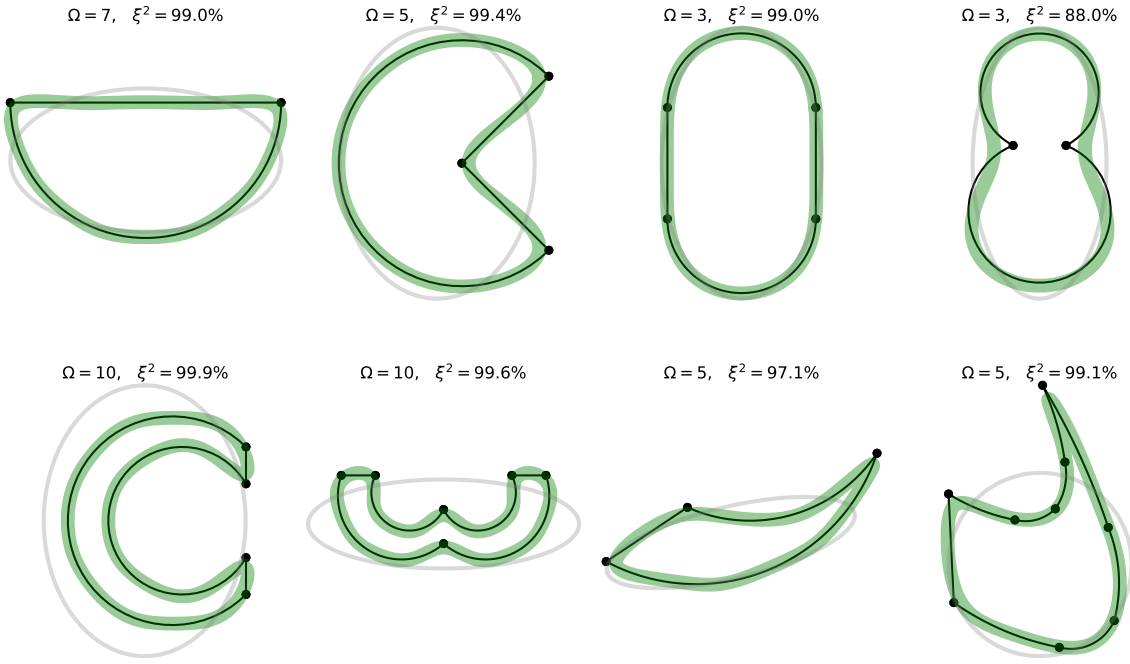

Fig. 6. Low frequency reconstruction $\mathcal{F}_\Omega$ (green) and covariance ellipse (gray) of illustrative piecewise-circular curves (black). Reconstruction accuracy is measured by the normalized ratio ξ defined in (23).

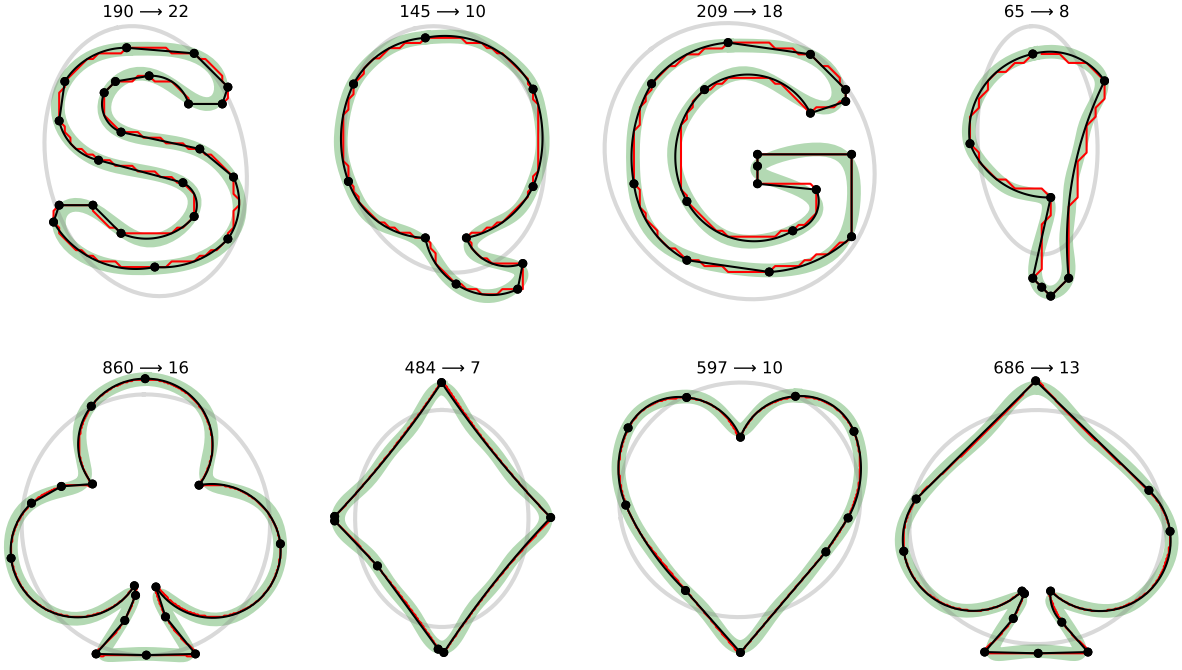

Fig. 7. Low frequency reconstruction $\mathcal{F}_{10}$ (light green) and covariance ellipse (gray) of piecewise-circular approximations (black) to digitized contours (red). The reduction in the number of nodes is indicated at the top of each diagram.

Simple polygonal approximations are usually suitable for low accuracy applications. Still, circular arcs are in general more effective, as shown in Fig. 8. The linear fragments become apparent in high frequency reconstructions (b). More importantly, a noticeable bias may appear in the low frequency coefficients (d) and moments (c) when, as usual, the nodes of the polygon are selected from the original curve. This has adverse effects for accurate alignment and shape normalization. In contrast, piecewise-circular approximations produce much better estimates for all frequencies and moments at a fraction of the cost.

6.1. Reproducible research

The source code for this work and *jupyter* notebooks with the experiments are freely available online[1].

7. Conclusion

Many natural and artificial shapes can be compactly represented by piecewise circular and linear curves. This model offers an excellent balance between analytic simplicity and accuracy, using several arcs to approximate fragments of variable curvature. We have developed practical algorithms for basic analysis tools, namely Fourier coefficients and moments, that can now be applied to more demanding applications at a fraction of the computational cost. For instance, Jacobians of descriptors extracted from deformable shapes, needed for optimization of alignment transformations, can be efficiently estimated on low cost devices. Future work includes an optimized implementation for visual navigation applications, and research on fast extraction of circular arcs on the fly from images.

Acknowledgments

This work was supported by the Spanish MINECO, as well as European Commission FEDER funds, under grant TIN2015-66972-C5-3-R.

References

Burkhardt, H., 2007. Calculating fourier coefficients of polygons. Lecture notes, University of Freiburg.
Chandrupatla, T.R., Osler, T.J., 2008. Approximating an ellipse with four circular arcs. Mathematics and Computer Education 42, 220.
Douglas, D.H., Peucker, T.K., 1973. Algorithms for the reduction of the number of points required to represent a digitized line or its caricature. Cartographica: The Int. J. for Geographic Inf. and Geovisualization 10, 112–122.
Hu, M.K., 1962. Visual pattern recognition by moment invariants. IRE Trans. Info. Theory IT-8, 179–187.
Kolesnikov, A., 2012. Segmentation and multi-model approximation of digital curves. Pattern Recognition Letters 33, 1171–1179.
Kolesnikov, A., Kauranne, T., 2014. Unsupervised segmentation and approximation of digital curves with rate-distortion curve modeling. Pattern Recognition 47, 623–633.
Meek, D.S., Walton, D.J., 1992. Approximation of discrete data by g1 arc splines. Computer-Aided Design 24, 301–306.
Meurer, A., Smith, C.P., Paprocki, M., Čertík, O., Kirpichev, S.B., Rocklin, M., Kumar, A., Ivanov, S., Moore, J.K., Singh, S., Rathnayake, T., Vig, S., Granger, B.E., Muller, R.P., Bonazzi, F., Gupta, H., Vats, S., Johansson, F., Pedregosa, F., Curry, M.J., Terrel, A.R., Roučka, v., Saboo, A., Fernando, I., Kulal, S., Cimrman, R., Scopatz, A., 2017. Sympy: symbolic computing in python. PeerJ Computer Science 3, e103.
Pei, S.C., Horng, J.H., 1996. Optimum approximation of digital planar curves using circular arcs. Pattern Recognition 29, 383–388.
Persoon, E., Fu, K.S., 1977. Shape discrimination using fourier descriptors. IEEE Transactions on systems, man, and cybernetics 7, 170–179.
Rosin, P.L., 1999. A survey and comparison of traditional piecewise circular approximations to the ellipse. Comp. Aided Geometric Design 16, 269–286.
Rosin, P.L., West, G.A., 1989. Segmentation of edges into lines and arcs. Image and Vision Computing 7, 109–114.
Ruiz, A., Lopez-de-Teruel, P.E., Fernandez-Maimo, L., 2017. Efficient planar affine canonicalization. Pattern Recognition 72, 236 – 253.

[1] `http://dis.um.es/~alberto/piecewise.html`

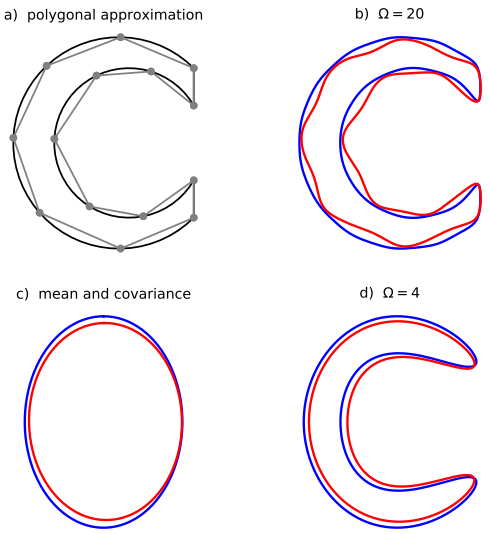

Fig. 8. Biased reconstruction and moments computed from a coarse polygonal approximation (red) vs ground truth (blue).

Safaee-Rad, R., Smith, K., Benhabib, B., Tchoukanov, I., 1992. Application of moment and fourier descriptors to the accurate estimation of elliptical-shape parameters. Pattern Recognition Letters 13, 497–508.

Sprinzak, J., Werman, M., 1994. Affine point matching. Pattern Recognition Letters 15, 337–339.

Tortorella, F., Patraccone, R., Molinara, M., 2008. A dynamic programming approach for segmenting digital planar curves into line segments and circular arcs, in: Pattern Recognition, 2008. ICPR 2008. 19th International Conference on, IEEE. pp. 1–4.

Wikipedia contributors, 2018. Integration by reduction formulae — Wikipedia, the free encyclopedia. `https://en.wikipedia.org/w/index.php?title=Integration_by_reduction_formulae&oldid=839028545`. [Online; accessed 6-May-2018].

Yang, S.N., Du, W.C., 1996. Numerical methods for approximating digitized curves by piecewise circular arcs. Journal of computational and applied mathematics 66, 557–569.

Zahn, C.T., Roskies, R.Z., 1972. Fourier descriptors for plane closed curves. IEEE Transactions on computers 100, 269–281.

Zhang, D., Lu, G., 2004. Review of shape representation and description techniques. Pattern Recognition 37, 1–19.